Binding of Zn−Chlorin to a Synthetic Four-Helix Bundle Peptide through Histidine Ligation

M. Reza Razeghifard* and Tom Wydrzynski

Photobioenergetics, Research School of Biological Sciences, The Australian National University, Canberra, ACT 0200, Australia

Received September 3, 2002; Revised Manuscript Received December 2, 2002

ABSTRACT: We have used a two histidine-containing synthetic peptide (Sharp et al. (1998) *Proc. Natl. Acad. Sci. U.S.A.* 95, 10465−10470) as a scaffold to bind Zn(II) chorin *e6* (ZnCe6) through histidine ligation. Protocols for the preparation and purification of the peptide using an *Escherichia coli* expression system are presented. Size-exclusion chromatography and circular dichroism measurements indicate that the peptide self-assembles into a four-helix bundle protein. Two variants of the peptide lacking either one or both of the histidine residues were used to demonstrate the stoichiometry of ZnCe6 binding. Comparison of the titration profiles determined by UV−vis spectroscopy for the purified one- and two-histidine peptides suggests that the two-histidine peptide can bind two ZnCe6. The binding stoichiometry of ZnCe6 was verified by gel chromatography and native gel electrophoresis using the peptide variant lacking histidine residues as the control. Like many other chlorophyll analogue molecules, ZnCe6 can be photooxidized. The light-induced electron transfer between the ZnCe6−peptide complex and the added phenyl-*p*-benzoquinone was measured using time-resolved EPR spectroscopy and shown to be faster and have a higher yield than the electron transfer between unbound ZnCe6 and quinone. The implications of constructing a ZnCe6−peptide complex in terms of artificial photosynthesis are discussed.

The plant and bacterial photosystems are the key complexes responsible for light-induced electron transfer in photosynthesis. These large pigment−protein complexes have evolved into multicomponent systems, which efficiently capture light energy and promote the directional transfer of electrons. In particular, the (bacterio)chlorophyll [(B)Chl][1] molecules at the reaction center are specialized to undergo photooxidation reactions, creating weak-to-strong oxidants while acting as primary electron donors. On the other hand, the (B) Chl molecules in the light-harvesting components serve only to collect and channel light energy to the reaction center. The unique difference in the functionality between the light harvesting and the reaction center (B)Chl's in the photosystems is entirely controlled by the protein environment, which provides not only a low-dielectric needed for the various reactions to occur but also the specific molecular interactions (such as metal coordination, hydrogen bonding, and hydrophobic interactions) that regulate the activity.

The application of site-directed mutagenesis to the natural photosystems has allowed for the experimental determination of some of the protein parameters that control the physicochemical properties of the bound (B)Chl's. For example, it was shown that the formation of up to four hydrogen bonds with the BChl special pair in *Rhodobacter sphaeroides* could additively increase the oxidation potential by a remarkable 355 mV (*1*, *2*). Interestingly, the increase in the midpoint potential was found to be dependent on the chemical nature of the H-bond forming residue, with histidine being the most effective. Likewise, the midpoint potential could be changed, but to a lesser extent, by introducing ionizable residues around the BChl special pair (*3*, *4*). In the case of metal coordination, by preparing a series of site-directed mutants at a histidine axial ligation site for the reaction center Chl of photosystem I (PSI), P_{700}, it was shown that the midpoint potential of $P_{700}^{\bullet+}/P_{700}$ could also be increased, in some cases by 140 mV (*5*). However, despite these successes, the use of *in vivo* site-directed mutants is often limited by the lower stability of the modified photosystems, making it difficult to obtain the high-resolution crystallographic measurements that are needed to interpret the details of a mutation effect. Nevertheless, a comprehensive modeling description of mutated bacterial reaction centers has recently been reported (*6*).

To fully understand the contribution of the protein elements to the physicochemical properties of protein-bound (B)Chl molecules, a model peptide with minimal complexity can provide valuable information. Unlike the natural system, a minimalist peptide scaffold can readily be modified to test the effect of a local environment change. However, analogues of (B)Chl are needed for such studies since it is difficult to design a binding pocket that can accommodate the phytyl tail of (B)Chl. In previous studies, (B)Chl analogues were covalently attached to the peptide. For example, a chemoselective method was used to covalently link a Chl derivative by an aldehyde group to a modified lysine residue in a

* Corresponding author. Phone: +61-(0)2-6125-3980. Fax: +61-(0)2-6125-8056. E-mail: razeghifard@rsbs.anu.edu.au.

[1] Abbreviations: (B)Chl, (bacterio)chlorophyll; Ce6, chlorin *e6*; CV, column volume; EPR, electron paramagnetic resonance; P_{680}, primary electron donor of PSII; P_{700}, primary electron donor of PSI; PPBQ, phenyl-*p*-benzoquinone; semi-PPBQ, semiquinone form of PPBQ; Tris, tris(hydroxymethyl)-aminomethane; PS (I or II), photosystem (I or II); ZnCe6, Zn(II) chorin *e6*.

10.1021/bi026787i CCC: $25.00
Published on Web 01/09/2003

synthetic four-helix bundle protein (*7*). Such chromoproteins offer a better-defined system but still lack the central metal ligation that is commonly provided by the protein backbone in the natural photosystems. In contrast to the rare reports on Chl analogue interactions, a series of elegant *de novo* heme protein maquettes have been successfully studied (for a review, see ref *8*). The development of such heme maquettes has been greatly aided by the recent advances in protein design, in which synthetic α-helical structures are created through rational or combinatorial approaches (for reviews, see refs *8*−*10*). In these instances, α-helical structures are obtained by engineering hydrophobic residues to align onto one side of a helical forming segment. This allows the hydrophobic residues to sequester themselves away from the aqueous solvent and to assemble an interior pocket that allows for the heme to bind. The exposed negatively and positively charged residues in the helical forming segment provides for stability and water solubility. It was thus clearly shown that synthetic peptide structures provide suitable environments for heme binding.

In addition, secondary electron donors and acceptor molecules have also been incorporated into synthetic peptides to promote stable electron transfers. For example, *de novo*-designed peptides containing ruthenium complexes, hemes, and flavins were used to study light-induced electron transfer within the peptide (*11*−*13*). Similarly, it was also shown that light-induced electron transfer could occur between a chromophore bound in the interior of a synthetic four-helix bundle protein and exogenously added anthraquinone (*14*). Likewise, electron transfer could be demonstrated across a noncovalently linked peptide−peptide interface in a dimeric 31-mer designed peptide (*15*). By varying the distance between two ruthenium ions attached to a three-helix bundle motif, a strong distance dependence for electron-transfer rate could be observed (*16*).

In this paper, we present our first study on synthetic peptides and show that Zn(II)−chlorin *e6* (ZnCe6) can ligate to histidine residues of a synthetic helix−loop−helix peptide originally designed by Dutton's group as a heme maquette. Three peptides were constructed that differ in respect to the number of histidine residues to show the crucial role of histidine ligation. We also present data on the flash-induced electron transfer between ZnCe6 bound to the synthetic peptide and an added quinone electron acceptor. We consider the ZnCe6−peptide complex as a starting point toward creating an artificial system to mimic the physicochemical properties of the natural photosystems.

EXPERIMENTAL PROCEDURE

Bacterial Expression. To express the peptide in *Escherichia coli*, an artificial gene encoding the peptide was first designed. The codon usage was optimized for *E. coli* to avoid rare codons and then randomized for overexpression. We used pET-32 Xa/LIC vector (Novagen, Inc.) to express the peptide as a fusion protein with thioredoxin, which protects the peptide from rapid proteolysis in *E. coli*. The vector is a linearized plasmid with about 16 base single-stranded overhangs for cloning. Ligation-independent cloning (LIC) is a very effective directional cloning that eliminates the need for restriction enzyme digestion or ligation reactions. The polymerase chain reaction (PCR) was used to make the peptide gene from three synthetic oligonucleotides with overlapping regions. To be able to insert the gene into the vector, complementary overhangs for the cloning site were also included as the extensions in the first and third oligonucleotides. The oligonucleotides were purchased from Sigma Genosys (Castle Hill, Australia). After initial cloning to NovaBlue competent cells, the circular plasmid was then transformed to *E. coli* strain BL21(DE3)pLysS for expression. The *E. coli* bacteria were grown in 12 L batches in LB medium inoculated with 200 mL of overnight grown culture at 37 °C. The growth medium was supplied with 100 μg/mL ampicillin and 34 μg/mL chloramphenicol. Expression was induced by the addition of isopropyl-D-thiogalactopyranoside (IPTG) to a final concentration of 1 mM after the culture reached an $OD_{600} = 0.5$. The cells were allowed to grow for 4 h and were then harvested by centrifugation at 5000*g* for 10 min at 4 °C.

Peptide Purification. The expressed fusion protein was purified using immobilized-metal affinity chromatography (IMAC) through chelation of the protein to a Ni−IDA fractogel matrix (Novagen, Inc.), making use of the His-tag that is encoded in a linker between the peptide and thioredoxin genes. The cell pellet was first resuspended in 500 mL of 50 mM Tris (pH 8.0) and 20% sucrose and incubated on ice for 10 min. The suspension was then centrifuged at 5000 rpm using a GS3 rotor at 4 °C. The pellet was gently resuspended in 500 mL of 50 mM Tris (pH 8.0) and incubated on ice for 10 min. The supernatants from both steps in the osmotic shock procedure were loaded onto 75 mL of Ni beads equilibrated with 50 mM Tris (pH 8.0), 5 mM imidazole, and 500 mM NaCl. The beads were washed with 10 column volumes (CV) of 50 mM Tris (pH 8.0), 50 mM imidazole, and 500 mM NaCl to remove the cellular proteins. The fusion protein was eluted from the column with 50 mM Tris (pH 8.0) and 250 mM imidazole. The pH of the protein solution was then adjusted to 5.0 using acetic acid and reloaded on a 50 mL CM-sepharose column (Pharmacia) to improve the purity. The column was washed with 20 CV of 50 mM acetate (pH 5.0) and 250 mM NaCl. The protein was eluted in 100 mL of 50 mM acetate (pH 5.0) and 550 mM NaCl. It was then concentrated on a 5 mL SP-sepharose column and eluted in 50 mM Tris (pH 8.0) and 1 M NaCl. The pure fusion protein was finally dialyzed against 10 mM Tris (pH 8.0) and 100 mM NaCl before cleavage. Protein concentrations were typically around 10 mg/mL. The peptide was efficiently cleaved from thioredoxin by a 96 h incubation with 1 unit of factor Xa (restriction grade, Novagen) per 500 μg of fusion protein at 37 °C in the presence of 100 μg/mL ampicillin. The cleavage specificity was confirmed by N-terminus sequencing of the peptide extracted from a SDS−PAGE gel by organic solvents. To purify the peptide from thioredoxin, the cleaved protein was first dialyzed against 10 mM Tris (pH 8.0) to remove the salt and then loaded on a 5 mL Q-sepharose column. The peptide was obtained by elution with 25 mM Tris (pH 8.0) and 50 mM NaCl, and it was shown to be free from thioredoxin by SDS−PAGE. The peptide samples were typically >95% pure as determined by reversed-phase C_{18} HPLC. The peptide concentrations were typically about 0.5 mM determined using $\epsilon_{280} = 5600\ M^{-1}\ cm^{-1}$.

ZnCe6 Preparation. Zn(II) chlorin *e6* was prepared by adding a 1:1 equiv of $Zn(OAc)_2$ to a solution of chlorin *e6*

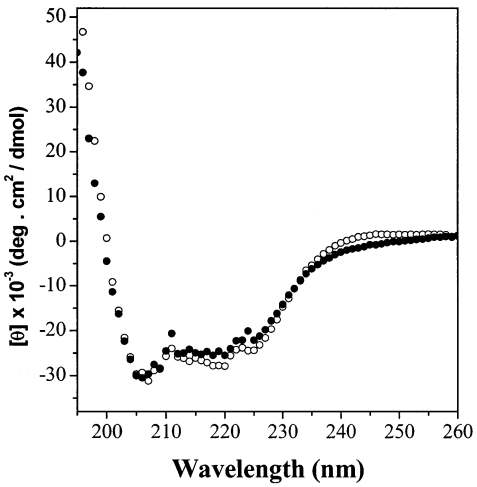

FIGURE 1: Far-UV CD spectra of 20 μM [H23H42] peptide in the absence (●) and the presence (○) of bound ZnCe6. The spectra were recorded in 25 mM glycine (pH 10) at 25 °C.

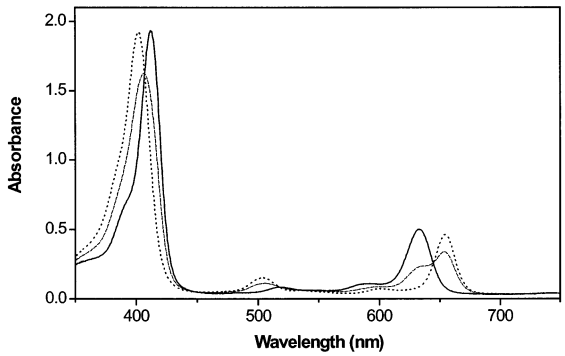

FIGURE 2: Optical spectra of 12.5 μM Ce6 (dashed line) in 25 mM glycine (pH 10) and after the addition of $Zn(OAc)_2$ (dash dotted line) at 1:1 ratio. The solid line represents the ZnCe6 spectrum after the completion of zinc insertion.

(Porphyrin Products) dissolved in 5 mM glycine, pH 10.0. The reaction was completed in 10 min as judged by the optical spectroscopy (see Figure 2). The prepared ZnCe6 was immediately purged under nitrogen, sealed, and stored at −70 °C.

UV−Vis Spectroscopy. Optical spectra were recorded on a Varian Cary 300 spectrophotometer. Titration experiments were performed by taking an individual 1 ms scan of the ZnCe6 spectrum for each added aliquot on an Olis RSM rapid scan spectrophotometer at room temperature. To accurately determine the Q_y peak position for each ZnCe6 concentration, the 20 highest absorbance points were averaged using Origin software.

Size-Exclusion Chromatography. Solution molecular mass was determined on a Waters FPLC system using a 600 × 10 mm Waters column packed with Superdex 200 beads (Pharmacia). The column was calibrated using horse heart cytochrome *c* (12 kDa) ribonuclease A (14 kDa), myoglobin (16 kDa), α-chymotrypsin (25 kDa), pepsin (35 kDa), and bovine serum albumin (67 kDa). The proteins were eluted in 25 mM glycine (pH 10) at a 0.5 mL/min flow rate and detected at 240 nm.

Pigment−Peptide Complex Purification. The pigment−peptide complex was purified from unbound pigment by size-exclusion chromatography using Superdex 200 beads. A 4-fold excess of ZnCe6 was added to 50 μL of peptide (0.4 mM) in 25 mM glycine (pH 10) and 50 mM NaCl and then loaded onto a 3 × 0.25 cm column. Upon passing the solution over the column, two green bands were separated as the unbound ZnCe6 is retained on the column.

Circular Dichroism (CD) Spectropolarimetry. CD spectra were recorded on an ISA Jobin Yvon CD 6 (Instruments S. A. Inc.) spectropolarimeter at room temperature using a 0.1 cm quartz cell. The peptide was dissolved in 25 mM glycine (pH 10) at 22 μM concentration.

EPR Spectroscopy. All EPR measurements were performed at room temperature on a Bruker ESP 300E spectrometer equipped with a TM011 cavity. Saturating 10 μs xenon flashes from an EG&G electrooptic flash lamp were used to excite the sample. A nonmagnetic optical fiber was used to illuminate the sample in the EPR cavity. The ESP 300E spectrometer computer controlled the EPR data acquisition and the triggering of the flash lamp. The flash lamp was triggered within a fixed delay time after the data acquisition was started. The electron-transfer kinetics were measured at the high-field peak of $ZnCe6^{\bullet+}$ EPR signal (g = 2.0010) using instrumental parameters of 100 kHz modulation frequency, 79 mW microwave power, 1 G modulation amplitude, and 20 μs time constant.

RESULTS

As a ZnCe6 binding scaffold, we have used one of the 63-residue synthetic peptides that were rationally designed by Dutton and co-workers (*12*). We have produced large quantities of the peptide using an *E. coli* expression system, with a typical yield of 20 mg/L. Taking advantage of the factor Xa protease activity, the peptide can be efficiently cleaved and purified from its fusion partner, with no unwanted residues. The peptide has the following amino acid sequence: MLKKLREE ALKLLEE FKKLLEE HLKWLE GGGGGGGG ELLKLH EELLKKC EELLKLA EERLKKL. We name the peptide [H23H42] in reference to the position of the two histidine residues. As indicated by the CD measurements in Figure 1 (●) the peptide contains a high α-helical content. It folds into a helix−loop−helix structure, in which each helix is comprised of approximately 3.5 modified heptad repeats (Leu Lys Lys Leu Leu Glu Glu). One cysteine and two histidine residues are appropriately located between the polar residues, while eight glycine residues provide a linkage for tight packing of the hydrophobic core (*17*). The histidine residues are placed adjacent to the glycine loop, toward the interior of the peptide. The placement of polar imidazole rings into the hydrophobic core causes some degree of destabilization, but the peptide maintains stable helices (*18*). Size-exclusion chromatography on a column calibrated with globular proteins showed that the peptides elute with an apparent molecular mass of 20 kDa (14.5 kDa is predicted for a dimeric form). The apparent molecular mass is consistent with the values found for this class of peptides (*19*) and clearly shows that the peptides self-assemble into four α-helix bundle proteins in aqueous solution. Although heme binding to the peptide has been well-characterized (for a review, see ref *8*), there are no equivalent studies involving metallo−chlorin complexes.

Figure 2 shows the optical spectra of Ce6 and ZnCe6 in 25 mM glycine (pH 10.0). A high pH was used to minimize pigment aggregation. Upon insertion of zinc into Ce6, a

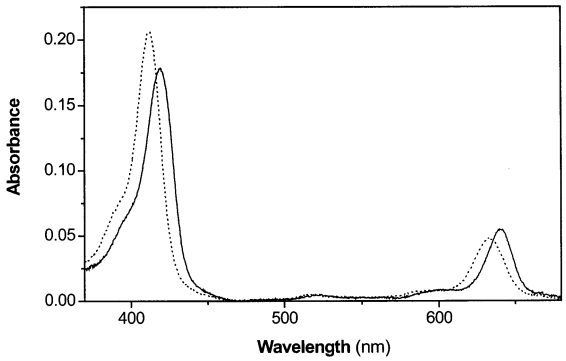

FIGURE 3: Optical spectra of 1.25 μM ZnCe6 free in solution (dashed line) and after addition of 12.5 μM [H23H42] peptide (solid line).

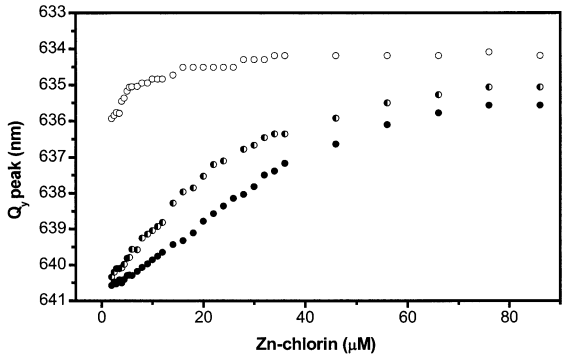

FIGURE 4: Spectrophotometric titration of ZnCe6 into 25 μM of the [H23H42] (●), [H23F42] (◐), and [F23F42] (○) peptides in 50 mM glycine (pH 10). The peak wavelength at the Q_y band is plotted against the ZnCe6 concentration.

significant 23 nm blue-shift and 10 nm red-shift occurs for Q_y and Soret bands positioning them at 633 and 411 nm, respectively, with a significant decrease in intensity in the Q_x region. On the basis of the four-orbital model, four $\pi \rightarrow \pi^*$ electronic transitions (a_{2u}, a_{1u}, e_{gx}, and e_{gy}) are predicted to give rise to the UV−vis absorption spectrum of metallo−chlorins (*20*, *21*). The Soret band components, B_x and B_y, are very intense and are theoretically very close in energy as they have not been resolved at room temperatures. On the other hand, the visible bands, weak Q_x and strong Q_y, are well-separated. In metallo−chlorins, Q_x is hardly discernible to experimentally allow monitoring of the interactions of the pigment with its environment.

Figure 3 shows the optical spectrum of ZnCe6 free in solution and ZnCe6 added to the [H23H42] peptide at a 1:10 ratio. There is a pronounced red shift and bandwidth change in the ZnCe6 spectrum in the presence of the peptide, which can be interpreted in terms of ZnCe6 incorporation into the peptide. In the Soret region, the 7 nm red-shift is accompanied by a 2 nm broadening causing a drop in the signal intensity, while the 8 nm red-shifted Q_y band is narrowed by 5 nm complemented with an increase in the signal intensity. The red-shift in the ZnCe6 spectrum in the presence of peptide is consistent with similar shifts characteristic of Chl bound to proteins (*22*, *23*). As a measure for ZnCe6 binding to the peptide, we have chosen to monitor the extent of the red shift in the Q_y band since this band allows unambiguous determination of ZnCe6 binding in the presence of heme, which has a very strong absorbance in the Soret region (see below).

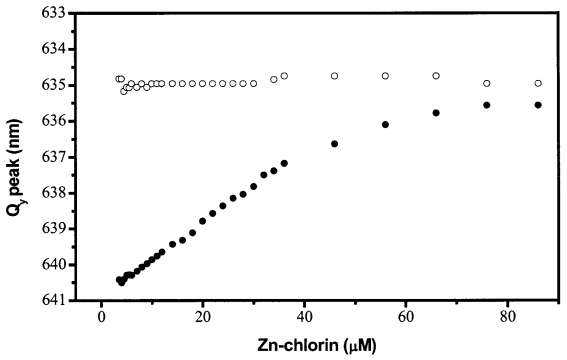

FIGURE 5: Spectrophotometric titration of ZnCe6 into 25 μM of the [H23H42] peptide (●) and the [H23H42] peptide premixed with 1:1 hemin (○). The peak wavelength at the Q_y band is plotted against the ZnCe6 concentration.

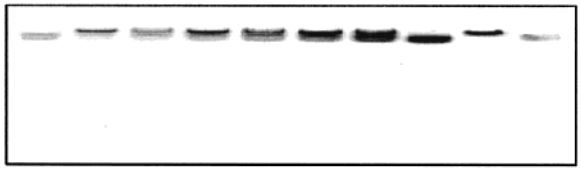

FIGURE 6: Native polyacrylamide gel electrophoresis of 5 μL of a 0.3 mM solution of the various peptides. Lanes 2, 4, and 6 are the [H23H42] peptide at 1:1, 1:2, and 1:3 ratios with ZnCe6. Lanes 3, 5, and 7 are the [F23F42] peptide at 1:1, 1:2, and 1:3 ratios with ZnCe6. Lanes 1 and 8 are the corresponding concentrations of ZnCe6 at the 1:1 and 1:3 ratios. Lane 9 is the [H23H42] peptide at a 1:1 ratio with hemin, and lane 10 is free hemin as a control.

Figure 4 (●) shows the titration profile upon binding ZnCe6 to the [H23H42] peptide using the red shift in the Q_y band. For these measurements, ZnCe6 was added stepwise to an aqueous solution of the peptide in 25 mM glycine (pH 10.0) and 25 mM NaCl. A high pH value above the PI of the peptide (pI = 7.2) was used to minimize electrostatic interactions between the ZnCe6 and the peptide and to prevent pigment aggregation. The results indicate that the incorporation of ZnCe6 into the peptide is spontaneous and saturates at a 2:1 molar ratio. To avoid long exposure of the sample to the detection light during the titration measurements, we used a rapid scan spectrophotometer capable of 1 ms scanning.

To show that ZnCe6 specifically interacts with the histidine residues of [H23H42], a variant of the peptide was made in which the two histidine residues were replaced with phenylalanine residues (i.e., [F23F42]). Replacement with phenylalanine was used to minimize conformational distortions to the peptide. As shown by Figure 4 (○), no comparable red shift is detected upon addition of ZnCe6 to the [F23F42] variant, clearly indicating that the ZnCe6 binding requires histidine. Similarly, hemin has been shown to bind to the [H23H42] peptide through bis ligation to the histidines (*24*). To show that ZnCe6 is associated with the same binding domain, ZnCe6 titration measurements were performed on the [H23H42] peptide premixed with the hemin in a 1:1 ratio. As shown in Figure 5, no red shift in the ZnCe6 Q_y band is detectable, strongly suggesting that hemin occupies the ZnCe6 binding site.

To verify the formation of a ZnCe6−[H23H42] complex, native gel electrophoresis was used. Figure 6 shows the gel pattern of the [H23H42] and [F23F42] peptides mixed with ZnCe6 in three different ratios, 1:1, 2:1, and 3:1 (lanes 2, 4,

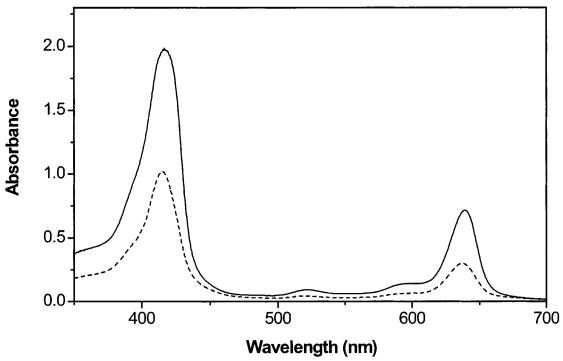

FIGURE 7: Optical spectrum of purified ZnCe6−[H23H42] complex (solid line) and the ZnCe6−[H23F42] complex (dashed line) normalized to 12.5 μM peptide concentration.

and 6 and lanes 3, 5, and 7, respectively). The gel electrophoresis was run under the same conditions as used in the titration experiments. The samples migrate on the gel since they are all negatively charged and separate according to size. Coomassie blue staining was used to visualize the peptide location. The ZnCe6−peptide complexes, which are larger than free ZnCe6, appear as a sharp dark bands suggesting that they are in a nonaggregating, homogeneous form. The free ZnCe6 appears as more diffuse bands that are displaced from the ZnCe6−peptide complexes. For comparison, samples of the hemin−[H23H42] complex (lane 9) and free hemin (lane 10) were also run on the same gel. Consistent with the small red shift observed in the titration data (Figure 4), the [F23F42] peptide shows some binding of ZnCe6 at the highest 3:1 ratio, but it is much less than with [H23H42] peptide. This residual effect is probably due to nonspecific association of ZnCe6 with [F23F42]. However, the presence of the histidines in the [H23H42] peptide dramatically increases the visual extent of ZnCe6 binding.

To show that both histidines can bind a ZnCe6 molecule, another peptide variant containing a single histidine (i.e., [H23F42]) was made. The titration measurements for the [H23F42] peptide are shown in Figure 4 (◐). Comparison of the slopes in the titration profiles indicates that the [H23H42] peptide binds twice as much ZnCe6 as the [H23F42] peptide. This result suggests that each histidine residue in the [H23H42] peptide can potentially ligate one ZnCe6 molecule. To estimate the dissociation constants (K_d) for ZnCe6 binding to the peptides, the bound fraction was calculated by deconvoluting spectra at each ZnCe6 concentration using two Gaussian functions derived from Figure 3 spectra parameters. The two independent K_d values of 0.35 and 1 μM were calculated for the ZnCe6 binding to each histidine of [H23H42] peptide. The K_d value of 0.4 μM for the ZnCe6 binding to the single histidine of [H23F42] peptide was also in the same range.

To confirm this stoichiometry, ZnCe6−[H23H42] and ZnCe6−[H23F42] peptide complexes were prepared in excess ZnCe6 and then isolated from the free ZnCe6 using size-exclusion chromatography. Figure 7 shows the optical spectra of the purified complexes for the [H23H42] and [H23F42] peptides normalized to the same peptide concentration estimated from the absorbance at 280 nm. On the basis of the peak intensities, it becomes evident that the [H23H42] peptide binds twice as much ZnCe6 as the [H23F42] peptide. The examination of ZnCe6−peptide

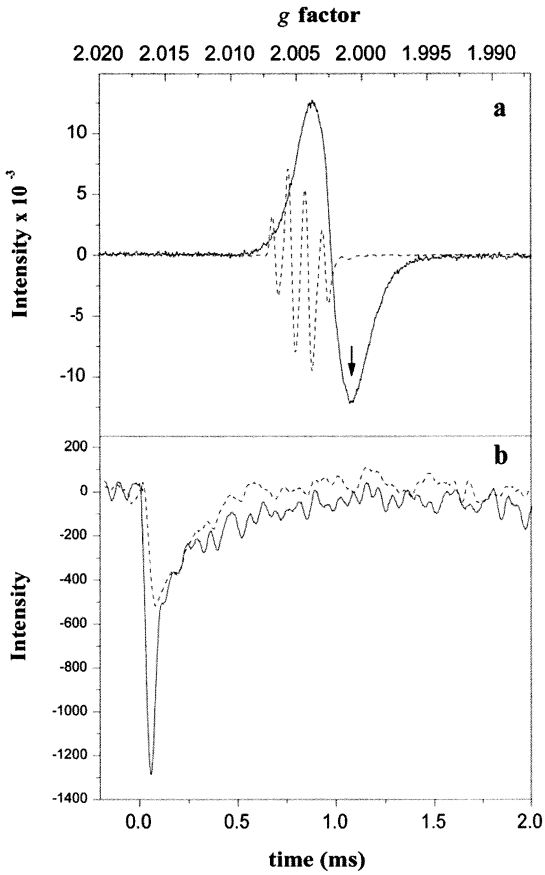

FIGURE 8: (a) X-band EPR spectra of 0.5 mM ZnCe6$^{\bullet+}$ and semi-PPBQ. Instrumental conditions are as follows: 100 kHz modulation frequency, 79 mW microwave power, 1 G modulation amplitude, and 40 ms time constant. The arrow indicates the field position where the kinetic measurements were taken. (b) The kinetic traces after repetitive flashing of the ZnCe6−[H23H42] complex (solid line) and free ZnCe6 (dashed line) in the presence of PPBQ. The signals were averaged over 6000 events.

complexes by gel permeation chromatography and CD spectroscopy (Figure 1, ○) confirmed that the four α-helix bundle architecture of protein was not significantly altered upon binding ZnCe6. This means that in the case of [H23H42] peptide, there are up to four ZnCe6 pigments associated with the $[H23H42]_2$ protein that represents the dimeric form. The apparent molecular mass of the ZnCe6−[H23H42] complex was determined as 23 kDa slightly higher than that obtained for the apo protein.

Like the natural Chl molecules, ZnCe6 can act as a light-activated electron donor (*25*). To reversibly photooxidize ZnCe6, and prevent irreversible photodamage, an appropriate cyclic electron acceptor/donor system (e.g., phenyl-*p*-benzoquinone, or PPBQ) needs to be coupled to ZnCe6 photooxidation. Since such redox active components carry unpaired electrons, EPR techniques can be used to monitor their kinetics of formation and decay (*26*, *27*). Figure 8a shows the EPR signals for semi-PPBQ (dashed line) and ZnCe6$^{\bullet+}$ (solid line) obtained under continuous flash illumination in aqueous solution. Electron transfer between ZnCe6 and the PPBQ can be measured unambiguously at the negative peak of ZnCe6 spectrum (arrow in Figure 8a) since the spectra of semi-PPBQ overlaps only with the positive peak of ZnCe6. Since very concentrated samples are needed for EPR measurements, ZnCe6 was added at a 1:3 ratio to the

[H23H42] peptide. At this ratio, it is likely that the complex carries only one ZnCe6 since the formation of the dimeric form will be energetically less favorable. Figure 8c shows the light-induced changes in the ZnCe6 EPR signal obtained by repetitive flashing of samples containing 0.1 mM ZnCe6 free (dashed line) or bound to the [H23H42] peptide (solid line) in the presence of 0.4 mM PPBQ. The sharp rise in the signals corresponds to the light-induced formation of the oxidized ZnCe6 cation radical through electron donation from the excited state to PPBQ forming the semi-PPBQ. Comparison of kinetics reveals a much faster (instrument-limited) rise in the presence of the [H23H42] peptide than for the free ZnCe6. On the other hand, the decay kinetics are virtually the same. Since this a two-component system, the electron ultimately returns from semiquinone to oxidized ZnCe6 through charge recombination. The at least doubling of the ZnCe6 signal intensity in the presence of [H23H42] suggests that the peptide provides a more suitable environment for the photooxidation of ZnCe6. A similar increase in the signal intensity was observed for the semi-PPBQ (data not shown).

DISCUSSION

There are probably two main factors that control the binding of ZnCe6 to the synthetic [H23H42] peptide (Figure 3). One is the axial ligation of the central metal ion in the chlorin molecule to the ϵ-nitrogen of histidine, and the other is the hydrophobic interaction between the aromatic rings of the chlorin head and the interior of the peptide. Through the use of two, one, and no histidine variants of the peptide (Figure 4), we have shown that histidine interactions strongly facilitate ZnCe6 binding. However, the type of metal center will have an effect on histidine ligation. For example, unlike Zn(II)-protoporphyrin that prefers five-coordination, six-coordinating Fe(III)-protoporphyrin binds tightly only to the two-histidine maquette because of bis ligation (*24*). Likewise, although Mg−BChl takes on penta-coordination similar to the natural Zn−BChl, it is known that Mg−BChl forms a tighter axial ligand than does Zn−BChl in bacterial reaction centers (*28*). Thus, one possible way to improve the binding affinity of chlorin to the [H23H42] peptide would be to use Mg−chlorin or a derivative.

With regard to hydrophobic interactions, the presence of noncoordinating hydrophobic residues flanking the coordinating histidine residue has been shown to increase heme binding to the synthetic peptide by >4.8 kcal/mol (*29*). As the surface area of the pigment can extend over 1 nm^2, it can potentially interact over broad hydrophobic patches of the peptide interior, extending up to two helix turns. The magnitude of the hydrophobic effect has been estimated to be 2.4 kcal/nm^2 and can thus be quite significant. Therefore, the other possible approach to increase the binding affinity of chlorin to the [H23H42] peptide would be to use more hydrophobic chlorin derivatives. However, preliminary results using trimethyl ester ZnCe6 and Zn(II) tetraphenylchlorin suggest that the buffering system needs to contain organic solvents or detergents to prevent pigment aggregation under conditions that would favor binding to the peptide. Indeed, it has been shown that for chlorophyll, which readily form aggregates in aqueous solution, buffering systems with detergent concentrations well above the critical micelle concentration have to be employed to prevent pigment aggregation (*30*). Similarly, detergents were used to reconstitute core light-harvesting complexes from peptides analogues of membrane-spanning segments and (B)Chls (*22*).

The stoichiometry determinations (Figures 4, 6, and 7) indicate that the two histidines in the [H23H42] peptide can bind up to two ZnCe6 molecules, under the conditions used, demonstrating that this class of peptides may potentially be used to create special dimers. In the natural photosystems, the special dimers are exitonically coupled with the distance and orientation between the chromophores being important factors. To create such a strong interacting dimer, the peptide design will need to be altered to change the relative histidine placements and increase the loop length to accommodate an interacting dimer binding pocket. Although dimer formation through axial ligation is rather difficult, it has been shown recently that a pair of covalently attached porphyrins with a strong split CD signal could be constructed between two α-helical peptides (*31*).

Unlike the Chl's that are labile and more difficult to work with, ZnCe6 is relatively more stable and in the presence of an electron acceptor can undergo repetitive photooxidation. Through making use of its physicochemical properties, we have demonstrated that a light-induced electron transfer can be established between ZnCe6 and exogenously added PPBQ (Figure 8). Interestingly, the [H23H42] peptide provides a more suitable environment for ZnCe6 oxidation as compared with free ZnCe6. The more efficient oxidation of the peptide-bound ZnCe6 could be a result of intra-protein electron transfer and specific structural distortions of ZnCe6 because of the peptide. Making use of native gel electrophoresis and gel chromatography, it was shown that a portion of PPBQ comigrated with the peptide (data not shown). This portion of quinone that is likely to be inside the hydrophobic patch of the peptide interior can be involved in intra-protein electron transfer. In the second plausible explanation, the distortions are mainly caused by the formation of hydrogen bonds and steric interactions between protein and pigment. These interactions have been shown to cause the movement of the metal ion relative to the macrocycle in Zn and Ni derivatives of BChl (*28*). The nonplanar conformational distortion of Chl molecules was clearly shown in the modified bacterial reaction centers as the result of mutation (*32*). Similarly, by analyzing the structure of more than 800 normal-coordinated heme groups from protein crystal structures, it has become evident that the protein also causes nonplanar distortions of heme (*33*, *34*). But the type and degree of distortion depends on the extent of protein−heme interaction. Conserved out-of-plane distortions of larger than 1 Å are found in some protein structures, in particular for *c*-type cytochromes and peroxidases.

The construction of a ZnCe6−peptide complex represents an attempt toward designing artificial peptides to mimic charge separation events in photosynthesis. In the photosystems for the charge separation to occur, the electron must be moved away from the oxidized primary electron donor in a series of fast and efficient short-range steps to prevent charge recombination. It is known that several different types of redox-active cofactors are involved in stabilizing the charge-separated state. Quinones and 4Fe-4S clusters are usually the stable electron acceptors, while a protein residue or a metal cofactor act as the immediate electron donor. As such, we are planning to introduce an electron donor into

the [H23H42] peptide by covalent attachment to the sole cysteine residue. Since the oxidation potential is greatly affected by protein interactions, various mutants will need to be tested to tune the redox activity, which can readily be made by redesigning and expressing the gene for [H23H42]. Some of the interactions that can be tested include H-bonding, as was recently shown to occur for the P_{700} special dimer of PSI (*35*). Although the current structural resolution of the P_{680} special dimer of PSII has not allowed exact determination of its local protein environment (*36*), the distortion of the macrocycle was suggested to contribute to the extremely high redox potential (*37*). Likewise, according to a computational model of PSII (*38*), it has been predicted that threonine and serine residues form hydrogen bonds and that a tryptophan residue interacts through van der Waals contacts with the porphyrin headgroup in controlling the redox properties of P_{680}. These are only some of the ways in which an artificial photosynthetic system can be created based on synthetic peptides.

ACKNOWLEDGMENT

We thank Mr. Sam Hay and Mr. Brett Wallace for many fruitful discussions and technical support in this study. We thank Mr. Nicholas Berrouard for technical assistance and Mr. Paul Gugger for CD measurements. The authors would also like to thank Dr. W. S. Chow for critical reading of the manuscript.

REFERENCES

1. Lin, X., Murchison, H. A., Nagarajan, V., Parson, W. W., Allen, J. P., and Williams, J. C. (1994) *Proc. Natl. Acad. Sci. U.S.A. 91*, 10265−10269.
2. Ivancich, A., Artz, K., Williams, J. C., Allen, J. P., and Mattioli, T. A. (1998) *Biochemistry 37*, 11812−11820.
3. Haffa, A. L. M., Lin, S., Katilius, E., Williams, J. C., Taguchi, A. K. W., Allen, J. P., and Woodbury, N. W. (2002) *J. Phys. Chem. B 106*, 7376−7384.
4. Johnson, E. T., and Parson, W. W. (2002) *Biochemistry 41*, 6483−6494.
5. Krabben, L., Schlodder, E., Jordan, R., Carbonera, D., Giacometti, G., Lee, H., Webber, A. N., and Lubitz, W. (2000) *Biochemistry 39*, 13012−13025.
6. Hughes, J. M., Hutter, M. C., Reimers, J. R., and Hush, N. S. (2001) *J. Am. Chem. Soc. 123*, 8550−8563.
7. Rau, H. K., Snigula, H., Struck, A., Robert, B., Scheer, H., and Haehnel, W. (2001) *Eur. J. Biochem. 268*, 3284−3295.
8. Gibney, B. R., and Dutton, P. L. (2001) *Adv. Inorg. Chem. 51*, 409−455.
9. DeGrado, W. F., Summa, C. M., Pavone, V., Nastri, F., and Lombardi, A. (1999) *Annu. Rev. Biochem. 68*, 779−819.
10. Moffet, D. A., and Hecht, M. H. (2001) *Chem. Rev. 101*, 3191−3203.
11. Mutz, M. W., McLendon, G. L., Wishart, J. F., Gaillard, E. R., and Corin, A. F. (1996) *Proc. Natl. Acad. Sci. U.S.A. 93*, 9521−9526.
12. Sharp, R. E., Moser, C. C., Rabanal, F., and Dutton, P. L. (1998) *Proc. Natl. Acad. Sci. U.S.A. 95*, 10465−10470.
13. Rau, H. K., DeJonge, N., and Haehnel, W. (1998) *Proc. Natl. Acad. Sci. U.S.A. 95*, 11526−11531.
14. Fahnenschmidt, M., Bittl, R., Schlodder, E., Haehnel, W., and Lubitz, W. (2001) *Phys. Chem. Chem. Phys. 3*, 4082−4090.
15. Kozlov, G. V., and Ogawa, M. Y. (1997) *J. Am. Chem. Soc. 119*, 8377−8378.
16. Mutz, M. W., Case, M. A., Wishart, J. F., Ghadiri, M. R., and McLendon, G. L. (1999) *J. Am. Chem. Soc. 121*, 858−859.
17. Suzuki, N., and Fujii, I. (1999) *Tetrahedron Lett. 40*, 6013−6017.
18. Gibney, B. R., Rabanal, F., Skalicky, J. J., Wand, A. J., and Dutton, L. P. (1999) *J. Am. Chem. Soc. 121*, 4952−4960.
19. Gibney, B. R., Rabanal, F., Reddy, K. S., and Dutton, P. L. (1998) *Biochemistry 37*, 4635−4643.
20. Hartwich, G., Fiedor, L., Simonin, I., Cmiel, E., Schäfer, W., Noy, D., Scherz, A., and Scheer, H. (1998) *J. Am. Chem. Soc. 120*, 3675−3683.
21. Singh, A., Huang, W.-Y., Egbujor, R., and Johnson, L. W. (2001) *J. Phys. Chem. A 105*, 5778−5784.
22. Meadows, K. A., Parkes-Loach, P. S., Kehoe, J. W., and Loach, P. A. (1998) *Biochemistry 37*, 3411−3417.
23. Satoh, H., Nakayama, K., and Okada, M. (1998) *J. Biol. Chem. 273*, 30568−30575.
24. Sharp, R. E., Diers, J. R., Bocian, D. F., and Dutton, P. L. (1998) *J. Am. Chem. Soc. 120*, 7103−7104.
25. Fukuzumi, S., Ohkubo, K., Imahori, H., Shao, J., Ou, Z., Zheng, G., Chen, Y., Pandey, R. K., Fujitsuka, M., Ito, O., and Kadish, K. M. (2001) *J. Am. Chem. Soc. 123*, 10676−10683.
26. Razeghifard, M. R., and Pace, R. J. (1999) *Biochemistry 38*, 1252−1257.
27. Razeghifard, M. R., Klughammer, C., and Pace, R. J. (1997) *Biochemistry 36*, 86−92.
28. Chen, L. X., Wang, Z., Hartwich, G., Katheder, I., Scheer, H., Scherz, A., Montano, P. A., and Norris, J. R. (1995) *Chem. Phys. Lett. 234*, 437−444.
29. Huffman, D. L., and Suslick, K. S. (2000) *Inorg. Chem. 39*, 5418−5419.
30. Eggink, L. L., and Hoober, J. K. (2000) *J. Biol. Chem. 275*, 9087−9090.
31. Tomizaki, K.-Y., Murata, T., Kaneko, K., Miike, A., and Nishino, N. (2000) *J. Chem. Soc., Perkin Trans. 2*, 1067−1074.
32. Ridge, J. P., Fyee, P. K., McAuley, K. E., van Brederode, M. E., Robert, B., van Grondelle, R., Isaacs, N. W., Cogdell, R. J., and Jones, M. R. (2000) *Biochem. J. 351*, 567−578.
33. Jentzen, W., Song, X.-Z., and Shelnutt, J. A. (1997) *J. Phys. Chem. B 101*, 1684−1699.
34. Jentzen, W., Ma, J.-G., and Shelnutt, J. A. (1998) *Biophys. J. 74*, 753−763.
35. Jordan, P., Fromme, P., Witt, H. T., Klukas, O., Saenger, W., and Krauss, N. (2001) *Nature 411*, 909−917.
36. Zouni, A., Witt, H.-T., Kern, J., Fromme, P., Krauss, N., Saenger, W., and Orth, P. (2001) *Nature 409*, 739−743.
37. Noguchi, T., Tomo, T., and Inoue, Y. (1998) *Biochemistry 37*, 13614−13625.
38. Svensson, B., Etchebest, C., Tuffery, P., van Kan, P., Smith, J., and Styring, S. (1996) *Biochemistry 35*, 14486−14502.

BI026787I